

Resonance decay effect on conserved number fluctuations in a hadron resonance gas model

D. K. Mishra,^{1,*} P. Garg,² P. K. Netrakanti,¹ and A. K. Mohanty^{†1}

¹*Nuclear Physics Division, Bhabha Atomic Research Center, Mumbai 400085, India*

²*Department of Physics and Astronomy, Stony Brook University,
SUNY, Stony Brook, New York 11794-3800, USA*

We study the effect of charged secondaries coming from resonance decay on the net-baryon, net-charge and net-strangeness fluctuations in high energy heavy-ion collisions within the hadron resonance gas (HRG) model. We emphasize the importance of including weak decays along with other resonance decays in the HRG, while comparing with the experimental observables. The effect of kinematic cuts on resonances and primordial particles on the conserved number fluctuations are also studied. The HRG model calculations with the inclusion of resonance decays and kinematical cuts are compared with the recent experimental data from STAR and PHENIX experiments. We find a good agreement between our model calculations and the experimental measurements for both net-proton and net-charge distributions.

PACS numbers: 25.75.Gz,12.38.Mh,21.65.Qr,25.75.-q,25.75.Nq

I. INTRODUCTION

Beam Energy Scan (BES) program at Brookhaven National Laboratory's Relativistic Heavy-Ion Collider (RHIC) has drawn much attention to explore the quantum chromodynamics (QCD) phase diagram in terms of temperature (T) and baryon chemical potential (μ_B) [1–4]. Several theoretical models suggest the existence of a critical point in the $T - \mu_B$ plane where the first order phase transition line originating from high μ_B ends [5–7]. The location of the critical point can be explored by systematically varying T and μ_B . Experimentally, one can vary the T and μ_B by varying the center of mass energy of the colliding ions. It has been suggested that the excitation function of conserved numbers like net-baryon, net-charge and net-strangeness fluctuations should show a non-monotonic behavior, as a possible signature of QCD critical end point (CEP) [8–10].

In the thermodynamic limit, the correlation length (ξ) diverges at CEP [1]. The moments of the net-baryon, net-charge, and net-strangeness distributions are related to the ξ of the system and hence these moments can be used to look for signals of a phase transition and critical point [11, 12]. Also, the comparison of experimentally measured cumulants with the lattice calculations enables us to extract the freeze-out parameters i.e. freeze-out temperature (T_f) and μ_B of the system produced in heavy-ion collisions [13–15]. In recent years, lots of efforts have been put on both theoretical and experimental fronts to study the fluctuation of conserved quantities. Current experiments at RHIC (PHENIX and STAR), have reported their measurements of higher moments for net-charge [15, 16] and for net-proton [17] multiplicity

distributions at different center-of-mass energies ($\sqrt{s_{NN}}$) using the data from BES. Experimentally, the net-baryon number fluctuations are not directly measured, as all the neutral baryons are not detected by most of the experiments. Hence, net-baryon fluctuations are accessible via measuring the net-proton distributions [18]. The net-charge fluctuations are accessible by measuring the stable charged particles such as pions, kaons and protons along with their anti particles [15, 16]. Similarly, the measurement of net-kaon acts as a proxy for net-strangeness fluctuations, as higher mass strange particles are not directly measured. There are several sources of non-equilibrium fluctuations, which can diminish the fluctuations measured by the experiments [19]. It is important to identify the non-critical baseline to understand the critical properties of different conserved number fluctuations.

Experimentally measured moments of the net distributions are related to the cumulants as: mean (M) = C_1 ; variance $\sigma^2 = C_2 = \langle(\delta N)^2\rangle$; skewness $S = C_3/C_2^{3/2} = \langle(\delta N)^3\rangle/\sigma^3$ and kurtosis $\kappa = C_4/C_2^2 = \langle(\delta N)^4\rangle/\sigma^4 - 3$, where N is the multiplicity of the distribution and $\delta N = N - M$. Hence, the ratios of the cumulants are related to the moments as: $\sigma^2/M = C_2/C_1$, $S\sigma = C_3/C_2$, $\kappa\sigma^2 = C_4/C_2$ and $S\sigma^3/M = C_3/C_1$. Further, the ratios of moments/cumulants can be related to the susceptibilities of n th order (χ^n) obtained from the lattice QCD or the HRG model calculations as $\sigma^2/M \sim \chi^{(2)}/\chi^{(1)}$, $S\sigma \sim \chi^{(3)}/\chi^{(2)}$, $\kappa\sigma^2 \sim \chi^{(4)}/\chi^{(2)}$, and $S\sigma^3/M \sim \chi^{(3)}/\chi^{(1)}$. One advantage of measuring the ratios is that the volume dependence on the experimental measured individual cumulants cancel out in the ratios. Experimentally, one measures only the final abundance of hadrons which includes both primordial particle production as well as contributions from the resonance decays. Production of resonances play important role for studying various properties of interaction dynamics in the heavy-ion collisions. Resonances having short life time which subsequently decays into stable hadrons and can affect the final hadron

[†]Presently at Saha Institute of Nuclear Physics, 1/AF, Bidhan nagar, Kolkata - 700064, India

*Electronic address: dkmishra@rcf.rhic.bnl.gov

yields and their number fluctuations.

The HRG model has been successful in explaining the particles produced in heavy ion collisions from AGS to LHC energies [20–22]. The susceptibilities and their ratios in hadronic phase calculated in the HRG model reasonably agrees with the lattice QCD results at lower μ_B [12]. Several studies have been performed with the HRG model for the fluctuation of conserved quantities, which are considered as baseline for such measurements [23–27]. Also, similar baseline studies have been performed using independent production model and transport model [28–31]. Keeping in mind the existence of CEP in the QCD phase diagram and the efforts put in both theoretical and experimental side, it is important to calculate the more appropriate baseline for comparison with the experimental data. In the present work, we estimate the contribution of resonances to the conserved number fluctuation using the HRG model. As discussed in Ref. [32], we also calculate the effect of average decay and by taking the higher order correlated terms, inclusion of weak decays in the model, the effect of different kinematic cuts on the resonance as well as on the primordial particles. It is important to consider the weak decays as many of the particles which are considered as stable in Ref. [32] decay before reaching the detector. For example, experimentally η^0 or Λ^0 particles are detected by reconstructing from their decayed daughters which are measured by the detector. Hence their contributions to the fluctuation of stable particles get influenced.

The paper is organized as follows: In the following section, we discuss the HRG model used in this study as well as the implementation of resonance decays. In Sec. III, the results for the observables $\chi^{(2)}/\chi^{(1)}$, $\chi^{(3)}/\chi^{(2)}$, $\chi^{(4)}/\chi^{(2)}$, and $\chi^{(3)}/\chi^{(1)}$ for considering different decay cases as well as inclusion of weak decays and effect of kinematical cuts are discussed. Section IV discuss the comparison of our model calculations to the experimental measurements. Finally, in Sec. V we summarize our findings and mention about the implication of this work.

II. HADRON RESONANCE GAS MODEL AND RESONANCE DECAYS

The partition function in the HRG model includes all relevant degrees of freedom of the confined, strongly interacting matter and contains all the interactions that result in resonance formation [25]. The heavy-ion experiments cover only a limited phase space, hence one can access only a part of the fireball produced in the collision which resemble with the Grand Canonical Ensemble [33]. Assuming a thermal system produced in the heavy-ion collisions, the thermodynamic pressure (P) can be written as sum of the partial pressures of all the particle

species i which may be baryon (B) or meson (M).

$$\frac{P}{T^4} = \frac{1}{VT^3} \sum_B \ln Z_i(T, V, \mu_i) + \frac{1}{VT^3} \sum_M \ln Z_i(T, V, \mu_i) \quad (1)$$

where

$$\ln Z_i(T, V, \mu_i) = \pm \frac{Vg_i}{2\pi^2} \int d^3p \ln \{1 \pm \exp[(\mu_i - E)/T]\}, \quad (2)$$

here T is the temperature, V is the volume of the system, μ_i is the chemical potential and g_i is the degeneracy factor of the i -th particle. The total chemical potential of the individual particle is $\mu_i = B_i\mu_B + Q_i\mu_Q + S_i\mu_S$, where B_i , Q_i and S_i are the baryon, electric charge and strangeness number of the i -th particle, with corresponding chemical potentials μ_B , μ_Q and μ_S , respectively. The $+ve$ and $-ve$ signs correspond to baryons and mesons respectively. In a static fireball, a particle of mass m , the volume element (d^3p) can be written as $d^3p = p_T m_T \cosh \eta dp_T d\eta d\phi$ and energy ($E = m_T \cosh \eta$) of the particle, where m_T is the transverse mass $= \sqrt{m^2 + p_T^2}$ with p_T , η and ϕ represents the transverse momentum, pseudo-rapidity and azimuthal angle, respectively. The experimental acceptances can be applied by considering the corresponding ranges in p_T , η and ϕ . The fluctuations of the conserved numbers are obtained from the derivative of the thermodynamic pressure with respect to the corresponding chemical potentials μ_B , μ_Q or μ_S . The n -th order generalized susceptibilities (χ) are written as;

$$\chi_x^{(n)} = \frac{d^n [P(T, \mu)/T^4]}{d(\mu_x/T)^n}. \quad (3)$$

For mesons χ_x can be expressed as

$$\chi_{x,meson}^{(n)} = \frac{X^n}{VT^3} \int d^3p \sum_{k=0}^{\infty} (k+1)^{n-1} \times \exp\left\{\frac{-(k+1)E}{T}\right\} \exp\left\{\frac{(k+1)\mu}{T}\right\}, \quad (4)$$

and for baryons,

$$\chi_{x,baryon}^{(n)} = \frac{X^n}{VT^3} \int d^3p \sum_{k=0}^{\infty} (-1)^k (k+1)^{n-1} \times \exp\left\{\frac{-(k+1)E}{T}\right\} \exp\left\{\frac{(k+1)\mu}{T}\right\}, \quad (5)$$

where X represents either B_i , Q_i or S_i of the i -th particle depending on whether the susceptibility χ_x represents for net-baryon, net-electric charge or net-strangeness. The total generalized susceptibilities will be the sum of susceptibility of mesons and baryons as $\chi_x^{(n)} = \sum \chi_{x,mesons}^{(n)} + \sum \chi_{x,baryons}^{(n)}$.

In the HRG model, at the chemical freeze-out time, all the particles (primordial as well as resonances) are in equilibrium. The collision energy dependence of freeze-out parameters (μ_B and T_f) are parametrized as given

in [21]. The energy dependence of μ_B is given as, $\mu_B(\sqrt{s_{NN}}) = 1.308 / (1 + 0.273 \sqrt{s_{NN}})$ and the μ_B dependence of freeze-out temperature is given as $T_f(\mu_B) = 0.166 - 0.139 \mu_B^2 - 0.053 \mu_B^4$. Further, the ratio of baryon to strangeness chemical potential on the freeze-out curve is parametrized as $\frac{\mu_S}{\mu_B} \simeq 0.164 + 0.018 \sqrt{s_{NN}}$. Similarly, the energy dependence of μ_Q and μ_S are parametrized as given in [25]. In the HRG model, after the production of all the particles, the resonances are allowed to decay to their corresponding daughter particles, hence contributing to the final abundance of the stable meson and baryon numbers. These decay daughters from the resonance can influence the fluctuation of the final hadrons. The ensemble averaged stable particle yield will have contribution from both primordial production and the resonance decay [23, 34],

$$\langle N_i \rangle = \langle N_i^* \rangle + \sum_R \langle N_R \rangle \langle n_i \rangle_R \quad (6)$$

where $\langle N_i^* \rangle$ and $\langle N_R \rangle$ correspond to the average primordial yield of particle species i and of the resonances R , respectively. The summation runs over all the resonances which decay to the final particle i and $\langle n_i \rangle_R = \sum_r b_r^R n_{i,r}^R$ is the average number of particle type i produced from the resonance R . Further, b_r^R is the branching ratio of the r -th decay channel of the resonance R and $n_{i,r}^R$ is the number of particle i produced in that decay branch. The generalized susceptibility for stable particle i of n -th order can be written as

$$\chi_i^{(n)} = \chi_i^{*(n)} + \sum_R \chi_R^{(n)} \langle n_i \rangle_R^n \quad (7)$$

The second term in Eq. 7 includes contributions from fluctuations of primordial resonances and average number of produced particle of type i . We follow Eqs. (17) - (20) from Ref. [32] to calculate the average contributions from the resonances, where we consider fluctuation in the resonance production only and the number of decay daughters are assumed to be fixed. In this work, we refer this as average decay contributions. For completeness we rewrite the same cumulant equations here as given in Ref. [32];

$$\langle (\Delta N_i)^2 \rangle = \langle (\Delta N_i^*)^2 \rangle + \sum_R \langle (\Delta N_R)^2 \rangle \langle n_i \rangle_R^2 \quad (8)$$

$$\langle (\Delta N_i)^3 \rangle = \langle (\Delta N_i^*)^3 \rangle + \sum_R \langle (\Delta N_R)^3 \rangle \langle n_i \rangle_R^3 \quad (9)$$

$$\langle (\Delta N_i)^4 \rangle = \langle (\Delta N_i^*)^4 \rangle + \sum_R \langle (\Delta N_R)^4 \rangle \langle n_i \rangle_R^4 \quad (10)$$

Resonance decay processes are probabilistic in nature, which itself causes the final particle number fluctuations. In above Eqs. (8)–(10), we use $\langle n_i \rangle$ which is same as the sum of the branching ratios of the different decay

branches of the resonance. But the number of decay products follow a random distribution which gives fluctuation in the final number of particles. Detailed discussion of resonance decay is given in Refs. [23, 24, 32]. After considering the fluctuation in the produced daughters, the modified cumulants in Eqs. (8)–(10) of the stable particle from the resonance contributions (full decay) can be written as [32];

$$\begin{aligned} \langle (\Delta N_i)^2 \rangle &= \langle (\Delta N_i^*)^2 \rangle + \sum_R \langle (\Delta N_R)^2 \rangle \langle n_i \rangle_R^2 \\ &+ \sum_R \langle N_R \rangle \langle (\Delta n_i)^2 \rangle_R \end{aligned} \quad (11)$$

$$\begin{aligned} \langle (\Delta N_i)^3 \rangle &= \langle (\Delta N_i^*)^3 \rangle + \sum_R \langle (\Delta N_R)^3 \rangle \langle n_i \rangle_R^3 \\ &+ 3 \sum_R \langle (\Delta N_R)^2 \rangle \langle n_i \rangle_R \langle (\Delta n_i)^2 \rangle_R \\ &+ \sum_R \langle N_R \rangle \langle (\Delta n_i)^3 \rangle_R \end{aligned} \quad (12)$$

$$\begin{aligned} \langle (\Delta N_i)^4 \rangle &= \langle (\Delta N_i^*)^4 \rangle + \sum_R \langle (\Delta N_R)^4 \rangle \langle n_i \rangle_R^4 \\ &+ 6 \sum_R \langle (\Delta N_R)^3 \rangle \langle n_i \rangle_R^2 \langle (\Delta n_i)^2 \rangle_R \\ &+ \sum_R \langle (\Delta N_R)^2 \rangle \left[3 \langle (\Delta n_i)^2 \rangle_R^2 \right. \\ &\left. + 4 \langle n_i \rangle_R \langle (\Delta n_i)^3 \rangle_R \right] \\ &+ \sum_R \langle N_R \rangle \langle (\Delta n_i)^4 \rangle_R \end{aligned} \quad (13)$$

Above Eqs. (11)–(13), which we refer as full decay, the fluctuation of the daughter particles are also considered along with the fluctuation of the resonances. If there is no correlation among the daughter particles, the fluctuation in the multiplicity calculated using Eqs. (11)–(13) will be very close to the average fluctuation contribution Eqs. (6)–(10) from resonance decay [32]. The higher order terms $\langle (\Delta n_i)^2 \rangle_R$, $\langle (\Delta n_i)^3 \rangle_R$, and $\langle (\Delta n_i)^4 \rangle_R$ will be zero for the resonances having only one decay channel or the number of species i is same in each decay branch. Hence, the higher order terms will have higher contribution for net-charge and net-kaon case with compared to net-proton. In this calculation, we have included mesons and baryons of mass up to 2.5 GeV as listed in the particle data book. We consider two different cases, one with weakly decaying particles regarded as stable and in another letting the weakly decaying particles decay into stable ones. In line with Ref. [32], for the first case, we have considered 26 weakly decaying particles as stable. By including weak decays in addition to the strongly decaying particles in our analysis, we observe substantial change on the values of cumulant ratios for all the conserved number which we will discuss in the following section.

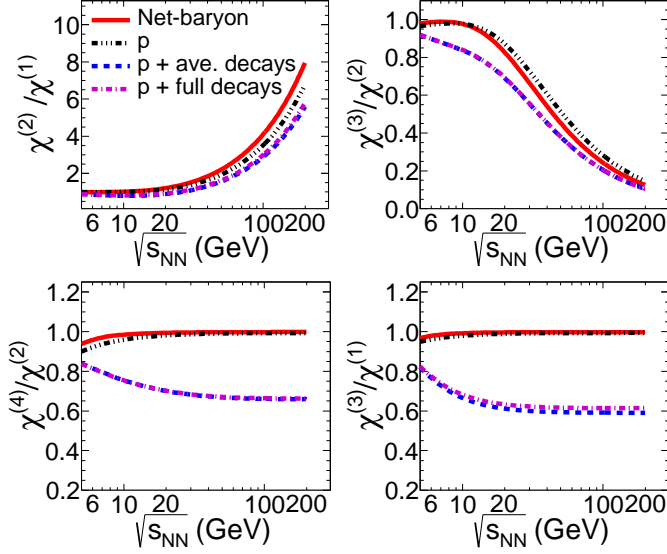


FIG. 1: Collision energy dependence of susceptibility ratios ($\chi^{(2)}/\chi^{(1)}$, $\chi^{(3)}/\chi^{(2)}$, $\chi^{(4)}/\chi^{(2)}$ and $\chi^{(3)}/\chi^{(1)}$) calculated in full phase space for net-baryons without resonance decay, primordial protons and primordial protons with resonance decay including weak decay resonances.

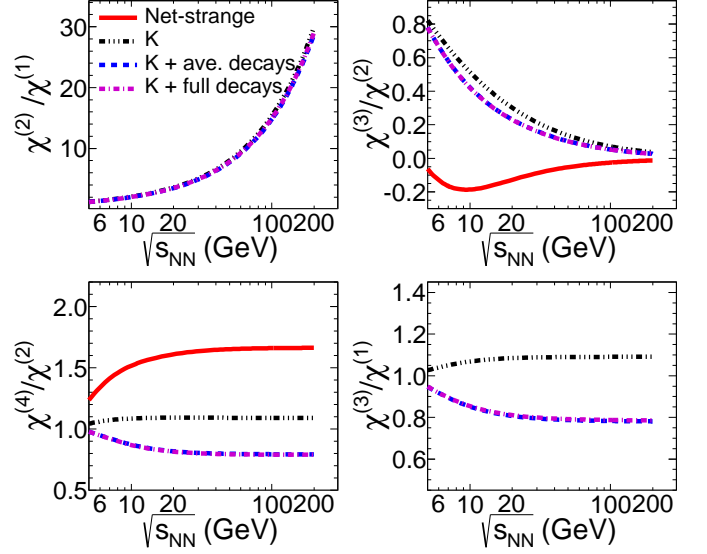


FIG. 3: Collision energy dependence of susceptibility ratios ($\chi^{(2)}/\chi^{(1)}$, $\chi^{(3)}/\chi^{(2)}$, $\chi^{(4)}/\chi^{(2)}$ and $\chi^{(3)}/\chi^{(1)}$) calculated in full phase space for net-strangeness without resonance decay, primordial kaons and primordial kaons with resonance decay including weak decay resonances.

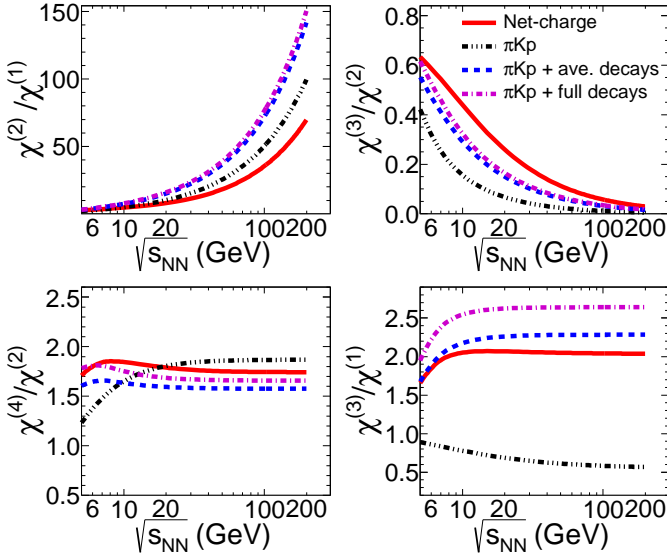


FIG. 2: Collision energy dependence of susceptibility ratios ($\chi^{(2)}/\chi^{(1)}$, $\chi^{(3)}/\chi^{(2)}$, $\chi^{(4)}/\chi^{(2)}$, and $\chi^{(3)}/\chi^{(1)}$) calculated in full phase space for net-charge without resonance decay, primordial charged particles (π, K, p) and primordial charged hadrons with resonance decay including weak decay resonances.

III. RESULTS AND DISCUSSION

Figures (1)–(3) show the variation of the susceptibility ratios for net-baryon, net-charge and net-strangeness

as a function of the collision energies by considering average decay (Eqs. (6)–(10)) and full decay contributions (Eqs. (11)–(13)) of resonances as discussed in previous section. Figure 1 shows ratios considering all the baryons including the resonances without decay, only primordial protons, primordial protons with average decay contributions from baryonic resonances using Eqs. (6)–(10) and primordial protons with contributions from fluctuation of resonances and their daughter particles (full decay) using Eqs. (11)–(13). Experimentally net-baryon fluctuations are accessible through net-proton fluctuations. There is significant effect of decay contributions observed with compared to no decay of resonances. However, the difference between average decay and full decay is negligible, which is in agreement with the findings of Ref. [32].

The net-charge fluctuations are accessible through measurement of fluctuation of stable charged particles (π, K and p). Figure 2 shows susceptibility ratios for net-charge which includes all the resonances without decay, only primordial stable charged particles (π, K and p), primordial particles with average decay contributions from the resonances using Eqs. (6)–(10) and primordial stable particles with full decay contributions using Eqs. (11)–(13). There is substantial change in the susceptibility ratios by including the resonance decay contributions, particularly for higher $\sqrt{s_{NN}}$ of $\chi^{(2)}/\chi^{(1)}$ and $\chi^{(3)}/\chi^{(2)}$ ratios for lower collision energies. The resonance decay effect for net-charge is larger as compared to net-baryon, because in case of baryons all the baryonic resonances decay into only one baryon in each decay branch, which is not the case for net-charge. Most of the higher mass

resonances decay into more than one charged particle. Also the higher mass resonances again decay into resonance which after few decay iterations decay into final stable hadrons. Further, the neutral resonances also contribute to the net-charge fluctuation. For example, ρ^0 meson which decays into $\pi^+\pi^-$ about 100%, if both the daughter particles will be accepted in the detector then the contribution to the mean of the net-charge from ρ^0 will be zero. In an ideal HRG model in the grand canonical ensemble, thermally produced and non-interacting particles and anti-particles are uncorrelated, hence the susceptibility of the net-conserved quantity is : $\chi_{net}^{(n)} = \chi_+^{(n)} + (-1)^n \chi_-^{(n)}$. The second and fourth or-

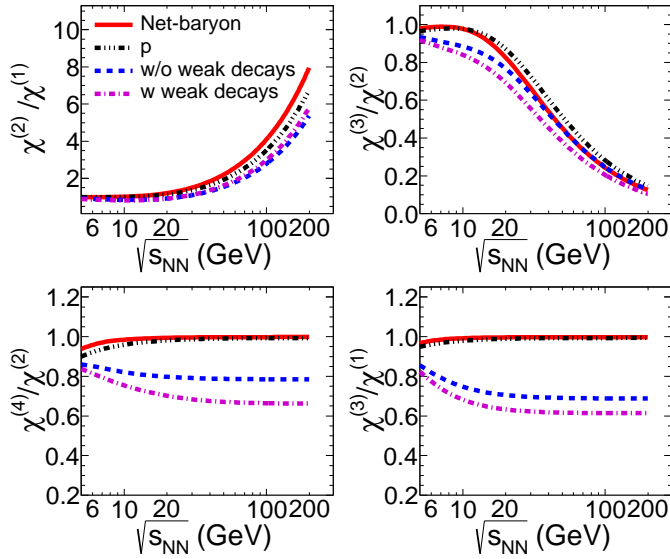


FIG. 4: Variation of susceptibility ratios ($\chi^{(2)}/\chi^{(1)}$, $\chi^{(3)}/\chi^{(2)}$, $\chi^{(4)}/\chi^{(2)}$ and $\chi^{(3)}/\chi^{(1)}$) as a function of $\sqrt{s_{NN}}$ calculated in full phase space for net-baryon without resonance decay, primordial proton, primordial proton with and without including weak decay in addition to the strongly decaying resonances.

der susceptibilities of ρ^0 will contribute to the net-charge susceptibility as the susceptibility of particle (π^+) and anti-particle (π^-) will get added. But the contribution of ρ^0 to the first and third order susceptibilities of the net-charge will be zero. This may be one reason why there is more effect of resonance decay in $\chi^{(2)}/\chi^{(1)}$ and $\chi^{(3)}/\chi^{(2)}$ ratios.

Experimentally, the net-strangeness fluctuations are accessible through measuring the net-kaon fluctuations. Figure 3 shows the susceptibility ratios of net-strange particles without resonance decay, considering only primordial kaons, primordial kaons with average decay contributions from the strange resonances using Eqs. (6)–(10) and primordial kaons with full decay contributions using Eqs. (11)–(13). For net-strangeness also there is significant resonance contributions observed in $\chi^{(3)}/\chi^{(2)}$ and $\chi^{(4)}/\chi^{(2)}$ ratios from the resonance decay with compared to no decay of resonances. We would like to men-

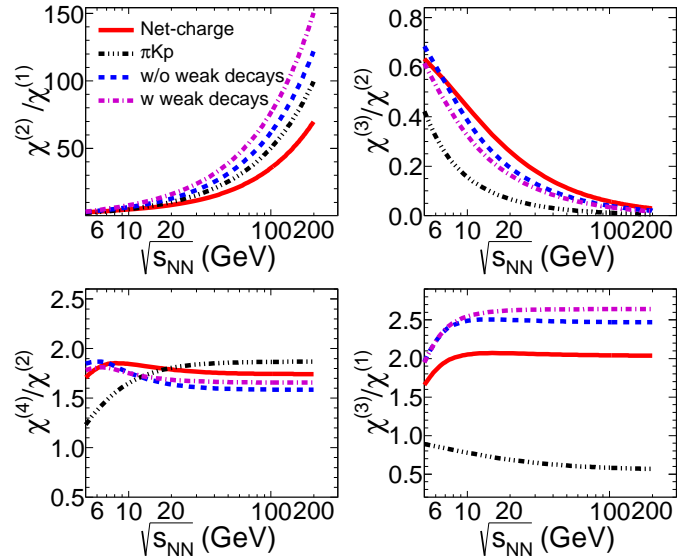


FIG. 5: Variation of susceptibility ratios ($\chi^{(2)}/\chi^{(1)}$, $\chi^{(3)}/\chi^{(2)}$, $\chi^{(4)}/\chi^{(2)}$ and $\chi^{(3)}/\chi^{(1)}$) as a function of $\sqrt{s_{NN}}$ calculated in full phase space for net-charge without resonance decay, primordial charged particles (π , K , p), primordial charged particles with and without including weak decay in addition to the strongly decaying resonances.

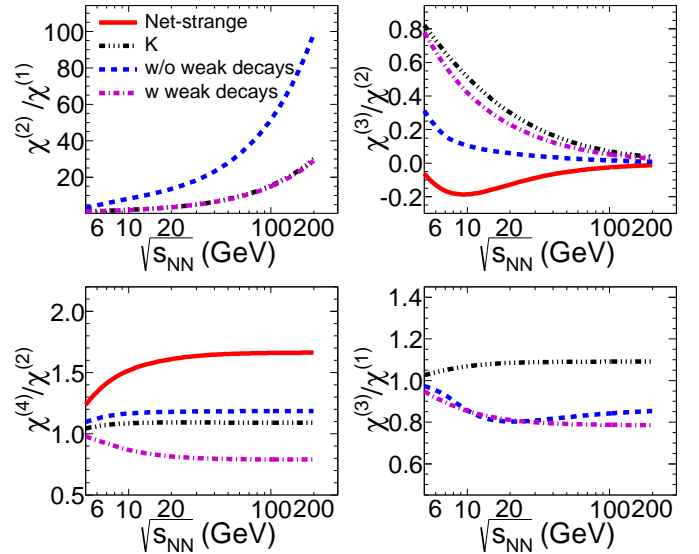


FIG. 6: Variation of susceptibility ratios ($\chi^{(2)}/\chi^{(1)}$, $\chi^{(3)}/\chi^{(2)}$, $\chi^{(4)}/\chi^{(2)}$ and $\chi^{(3)}/\chi^{(1)}$) as a function of $\sqrt{s_{NN}}$ calculated in full phase space for net-strange without resonance decay, primordial kaons, primordial kaons with and without including weak decay in addition to the strongly decaying resonances.

tion here that, the mean of the net-strangeness multiplicity is zero due to the imposed strangeness neutrality and iso-spin asymmetry in the initial state of Au + Au collisions [25]. Therefore, $\chi^{(2)}/\chi^{(1)}$ and $\chi^{(3)}/\chi^{(1)}$ diverges

in case of net-strange multiplicity distributions in HRG model, which are not shown in the Fig. 3.

Figures (4)–(6) show the energy dependence of susceptibility ratios for net-baryon, net-charge and net-strangeness. Figure 4 shows the susceptibility ratios for net-baryon without resonance decay, primordial net-protons, net-protons from primordial and resonance contributions without weak decays and including weak decay particles in addition to the resonance contributions from strong decay. The resonance decay contributions are calculated using full decay contributions using Eqs. (11)–(13). We consider K^0 , \bar{K}^0 , η^0 , Λ^0 , Σ^\pm , Σ^0 , Ξ^- , Ξ^0 , Ω^- and their anti-particles as weak decay particles. In Ref. [32], these particles were considered as stable particles and only strongly decaying particles were considered in the resonance decay. In the present work we have explicitly considered their weak decays in addition to the strongly decaying particles. There is very small effect in $\chi^{(2)}/\chi^{(1)}$ ratio for all the energies, but the $\chi^{(3)}/\chi^{(2)}$, $\chi^{(4)}/\chi^{(2)}$ and $\chi^{(3)}/\chi^{(1)}$ ratios further decrease at all $\sqrt{s_{NN}}$ as compared to the values of excluding weak decays. Similarly, Fig. 5, shows the susceptibility ratios for net-charge without decay of resonances, primordial π , K , p , and contributions from strongly decaying resonances along with and without weak decays. There is visible difference between the results with and without inclusion of weak decays. Figure 6, shows the susceptibility ratios for net-strangeness without decay of resonances, only primordial kaons, with and without inclusion of weak decays in addition to contribution from strongly decaying resonances. There is significant difference of the susceptibility ratios for with and without inclusion of weak decay contributions except $\chi^{(3)}/\chi^{(1)}$ ratio. For all the cases, net-baryon, net-charge and net-strangeness, it is important to consider weak decays contributions in addition to the strongly decaying particles while comparing model calculations with the experimental observables. Without decay of resonances and primordial contributions in Figs. (4)–(6) are same as shown in Figs. (1)–(3).

Figures (7)–(9) show the variation of susceptibility ratios as a function of $\sqrt{s_{NN}}$ for various p_T acceptances for net-baryon, net-charge and net-strangeness. The ratios without resonance decay are also shown for comparison. The p_T acceptance cuts have been applied to the stable particles only and the resonances are taken in full p_T range. We have also shown another case where p_T cut is applied to all the particles (stable as well as resonances). Although there is significant difference between with and without resonance decay, the p_T acceptance has very minimal effect on the susceptibility ratios after inclusion of resonance decay for all the conserved quantities. In Ref. [26], which was studied without taking resonance decay into account, a clear p_T dependence was observed for net-charge and net-strangeness cases at all collision energies. In reality the acceptance cuts should be applied separately on the daughters of resonances. The resonance may be produced in full acceptance which can

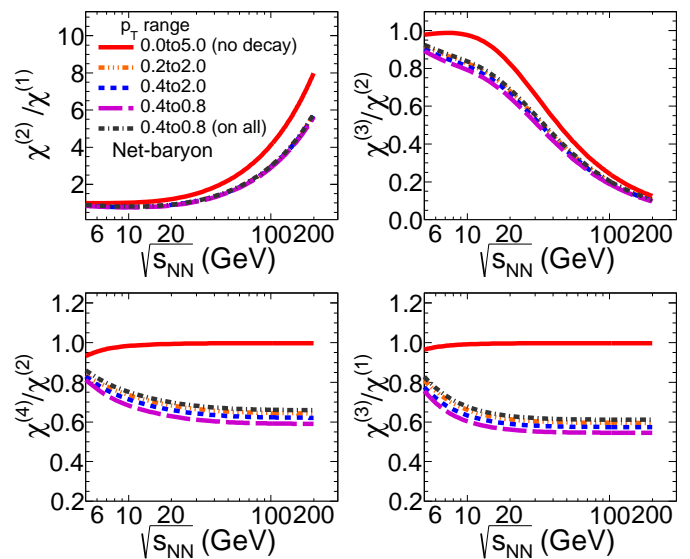


FIG. 7: Collision energy dependence of susceptibility ratios ($\chi^{(2)}/\chi^{(1)}$, $\chi^{(3)}/\chi^{(2)}$, $\chi^{(4)}/\chi^{(2)}$ and $\chi^{(3)}/\chi^{(1)}$) for net-protons for different p_T acceptances within $|\eta| < 0.5$. The results are for primordial protons with resonance decay including weak decay resonances.

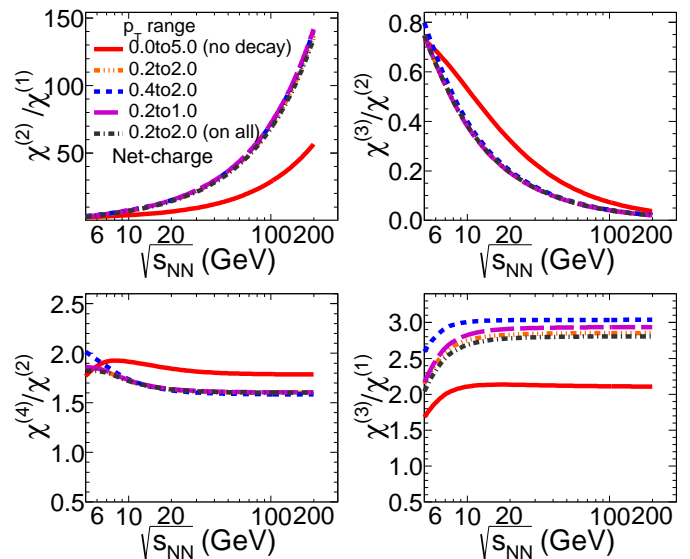


FIG. 8: Collision energy dependence of susceptibility ratios ($\chi^{(2)}/\chi^{(1)}$, $\chi^{(3)}/\chi^{(2)}$, $\chi^{(4)}/\chi^{(2)}$ and $\chi^{(3)}/\chi^{(1)}$) for net-charge for different p_T acceptances with $|\eta| < 0.5$. The results are for primordial charged particles (π , K , p) with resonance decay including weak decay resonances.

be outside the experimental acceptance, still the decay daughters have a chance to be accepted within the experimental acceptance because of their decay kinematics. It has been mentioned in Ref. [32] that, due to the elastic scatterings in thermally equilibrated hadronic phase, the

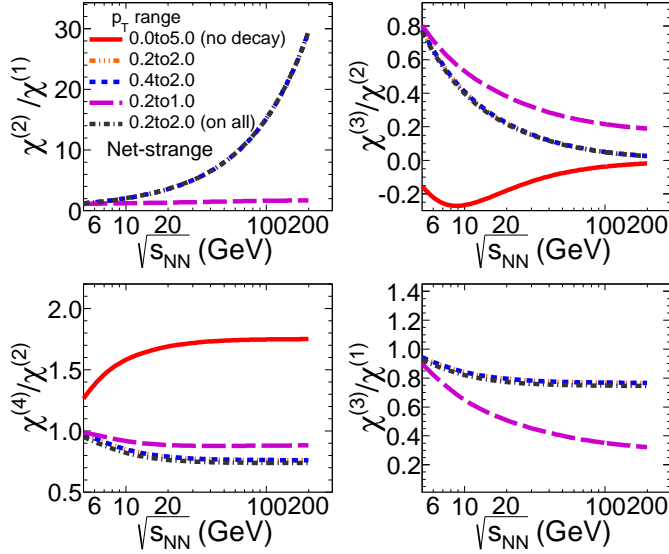


FIG. 9: Collision energy dependence of susceptibility ratios ($\chi^{(2)}/\chi^{(1)}$, $\chi^{(3)}/\chi^{(2)}$, $\chi^{(4)}/\chi^{(2)}$ and $\chi^{(3)}/\chi^{(1)}$) for net-kaons for different p_T acceptances within $|\eta| < 0.5$. The results are for primordial kaons with resonance decay including weak decay resonances.

kinematic cuts affect the same manner for the primordial particle and anti-particle from the resonance decay. However, this may not be true when the detector will have asymmetric azimuthal acceptance.

IV. COMPARISON TO THE EXPERIMENTAL MEASUREMENTS

Experimentally measured moments (M , σ , S , κ) of the net distributions are related to the susceptibilities as: $\sigma^2/M \sim \chi^{(2)}/\chi^{(1)}$, $S\sigma \sim \chi^{(3)}/\chi^{(2)}$, $\kappa\sigma^2 \sim \chi^{(4)}/\chi^{(2)}$. Figure 10 shows the energy dependence of σ^2/M , $S\sigma$ and $\kappa\sigma^2$ of net-proton distribution for central (0–5)% Au + Au collisions measured by STAR experiment [17]. The experimental data is studied within mid-rapidity ($|y| < 0.5$) and p_T range 0.4 to 0.8 GeV/c. The data is compared with the HRG calculations with no decay of resonances, only primordial protons, resonance decay with and without inclusion of weak decay contributions in addition to the contribution from strongly decaying resonances within the same experimental acceptance. We would like to mention here that, we have applied same p_T acceptance cuts to the primordial as well as resonances. The HRG calculations without resonance decay fail to explain σ^2/M at higher collision energies and $S\sigma$ values at lower $\sqrt{s_{NN}}$. The σ^2/M values are well described by considering only primordial protons but over estimates the $S\sigma$ and $\kappa\sigma^2$ values. The σ^2/M calculated in HRG with resonance decay along with inclusion of weak decay contributions are closer to the experimental values. The

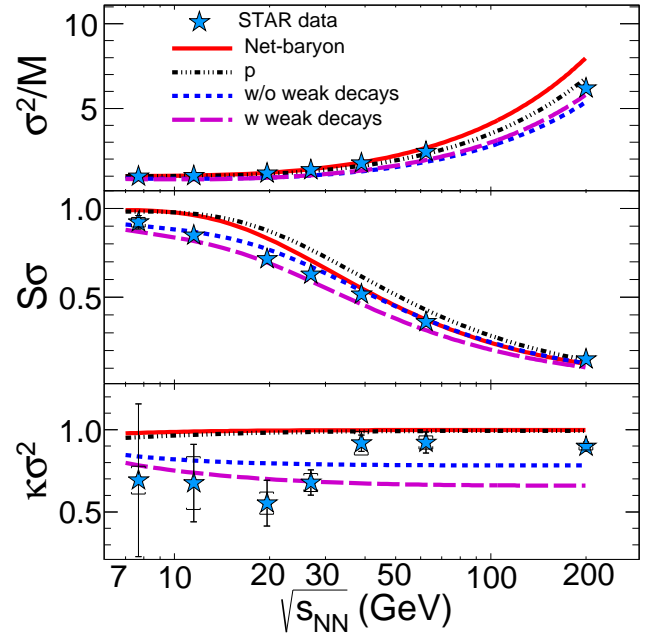


FIG. 10: The collision energy dependence of σ^2/M , $S\sigma$, and $\kappa\sigma^2$ of the net-baryon calculated using HRG model including resonance decay contributions. The model calculations are compared with the experimental net-proton cumulant ratios for most central (0–5)% Au + Au collisions by STAR experiment.

$S\sigma$ values lies between resonance decays with and without inclusion of weak decays. The $\kappa\sigma^2$ values at lower $\sqrt{s_{NN}}$ are better described by inclusion of weak decays. For higher collision energy (above 30 GeV), the HRG model under predict the experimental values. This may be because of the regeneration of the resonances at higher collision energies as observed in Refs. [32, 35]. Hence it is important to consider the weak decays in addition to the strongly decaying resonances in the HRG model while comparing with experimental data.

Figure 11 shows the energy dependence of σ^2/M , $S\sigma$ and $\kappa\sigma^2$ of net-charge distributions for most central (0–5)% Au + Au collisions within $|\eta| < 0.5$ and p_T range within 0.2 to 2.0 GeV/c measured by STAR experiment [16]. The experimental net-charge results are compared with the HRG calculations considering without resonance decay, only charged stable particles (π , K , p), resonance decay with and without inclusion of weak decays along with strongly decaying resonances. The HRG results for σ^2/M without resonance decay and considering only primordial particles shows lower values with compared to the experimental data. Where as the HRG calculations with resonance decay over estimates the experimental data. Inclusion of weak decays further worsen the agreement with the experimental data at higher $\sqrt{s_{NN}}$. The experimental $S\sigma$ and $\kappa\sigma^2$ values are explained by all cases of HRG because of the large uncertainties in the measured experimental data.

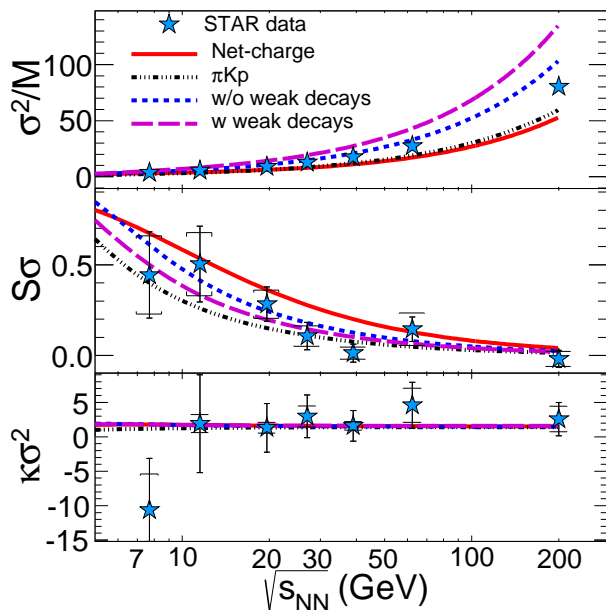


FIG. 11: The collision energy dependence of σ^2/M , $S\sigma$, and $\kappa\sigma^2$ of the net-charge calculated using HRG model including resonance decay contributions. The model calculations are compared with the experimental net-charge cumulant ratios for most central (0–5)% Au + Au collisions by STAR experiment.

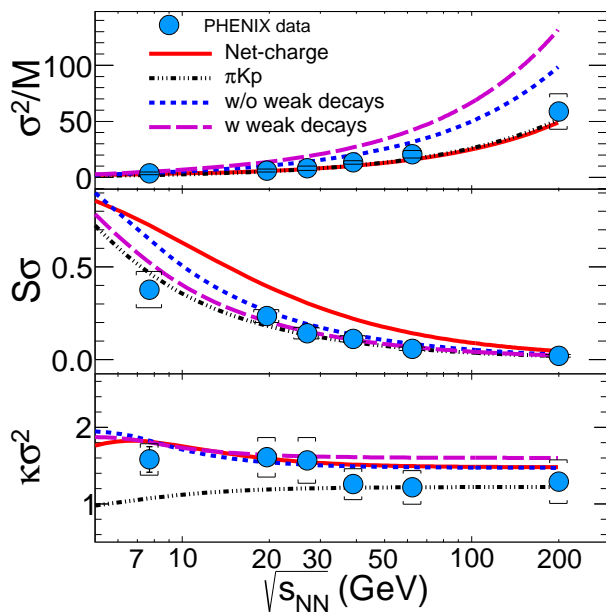


FIG. 12: The collision energy dependence of σ^2/M , $S\sigma$, and $\kappa\sigma^2$ of the net-charge calculated using HRG model including resonance decay contributions. The model calculations are compared with the experimental net-charge cumulant ratios for most central (0–5)% Au + Au collisions by PHENIX experiment.

Figure 12 shows the collision energy dependence of σ^2/M , $S\sigma$ and $\kappa\sigma^2$ of net-charge distribution for most central bin (0–5)% in Au + Au collisions measured by PHENIX experiment [15]. The experimental measurements are within $|\eta| < 0.35$ and p_T between 0.3 – 2.0 GeV/c. The experimental data are compared with the HRG calculations considering no decay of resonances, only primordial charged hadrons (π , K , p), with and without inclusion of weak decays in the resonance decay. The kinematic acceptance cuts applied to the HRG calculations are same as in experimental data. As observed in STAR net-charge results, the HRG calculations without resonance decay are more close to the experimental σ^2/M values. Inclusion of resonance decay over estimate the experimental data. Inclusion of weak decay in the resonance decay further deviates from the experimental values. The disagreement in σ^2/M between experimental data and the HRG may be because of the acceptance cuts. As mentioned before, we have applied the kinematic acceptance cuts on the resonance not on their daughter particles. Although, if we consider the resonances in full phase space for a 4π detector then the neutral resonances will not contribute to the net-charge fluctuations. For example the case ρ^0 , K^{*0} or Λ^0 , if we measure the daughter particles in full phase space, they will also not contribute to the net-charge fluctuation. This may be one of the reason, why σ^2/M are not explained by HRG model with resonance decay. The HRG calculations without resonance decay fails to explain the experimental $S\sigma$ at all $\sqrt{s_{NN}}$. The $S\sigma$ are well explained by resonance decay with weak decay contributions. In this case also, results from only primordial charged particles are more close to the experimental data. The $\kappa\sigma^2$ values are well explained by HRG with resonance decay within the experimental uncertainties at all the studied energies. The $\kappa\sigma^2$ values without resonance decay also shows similar results as with resonance decay. However, considering only primordial charged particles explain the experimental data very well at higher $\sqrt{s_{NN}}$ but fails to explain at lower collision energies.

V. SUMMARY

In conclusion we have studied the effect of resonance decay on conserved number fluctuations using a hadron resonance gas model. There is a significant effect of resonance decay as compared to no decay of resonances for all the conserved number fluctuations. The effect of considering primordial particles with average decay contributions of the resonances are studied. There is small effect whether we consider average decay or full decay of resonances. The inclusion of weak resonance decays in addition to the strongly decaying particles show visible difference compared to without inclusion of weak decays. The effect of different p_T acceptance cuts on the resonance decay are very minimal for all the conserved numbers. The experimental data for net-proton and net-

charge are compared with the HRG calculations, which are estimated within the similar kinematic acceptance as in the experiment. The cumulant ratios of net-proton distributions are better explained by considering the resonance decay contributions and the agreement further improves by inclusion of weak resonance decays. The HRG calculations for net-charge with resonance decay

over estimates the experimental σ^2/M values. However, the $S\sigma$ and $\kappa\sigma^2$ of net-charge experimental values are well explained by HRG calculations with resonance decay, which further improves by including the weak decays. Hence, it is important to consider resonance decays and with weak decay resonance contribution before comparing the model calculations with experimental data.

-
- [1] M. A. Stephanov, K. Rajagopal and E. V. Shuryak, Phys. Rev. Lett. **81**, 4816 (1998).
- [2] M. G. Alford, K. Rajagopal and F. Wilczek, Phys. Lett. B **422**, 247 (1998).
- [3] M. A. Stephanov, Phys. Rev. Lett. **76**, 4472 (1996).
- [4] Y. Aoki, G. Endrodi, Z. Fodor, S. D. Katz and K. K. Szabo, Nature **443**, 675 (2006).
- [5] M. A. Stephanov, Prog. Theor. Phys. Suppl. **153**, 139 (2004), Int. J. Mod. Phys. A **20**, 4387 (2005).
- [6] Z. Fodor and S. D. Katz, JHEP **0404**, 050 (2004).
- [7] M. A. Stephanov, K. Rajagopal and E. V. Shuryak, Phys. Rev. D **60**, 114028 (1999).
- [8] V. Koch, A. Majumder and J. Randrup, Phys. Rev. Lett. **95**, 182301 (2005).
- [9] M. Asakawa, U. W. Heinz and B. Muller, Phys. Rev. Lett. **85**, 2072 (2000).
- [10] M. Asakawa, S. Ejiri and M. Kitazawa, Phys. Rev. Lett. **103**, 262301 (2009).
- [11] S. Ejiri, F. Karsch and K. Redlich, Phys. Lett. B **633**, 275 (2006).
- [12] A. Bazavov, H. T. Ding, P. Hegde, O. Kaczmarek, F. Karsch, E. Laermann, S. Mukherjee and P. Petreczky *et al.*, Phys. Rev. Lett. **109**, 192302 (2012).
- [13] S. Borsanyi, Z. Fodor, S. D. Katz, S. Krieg, C. Ratti and K. K. Szabo, Phys. Rev. Lett. **113**, 052301 (2014).
- [14] P. Alba, W. Alberico, R. Bellwied, M. Bluhm, V. Mantovani Sarti, M. Nahrgang and C. Ratti, Phys. Lett. B **738**, 305 (2014).
- [15] A. Adare *et al.* [PHENIX Collaboration], Phys. Rev. C **93**, 011901 (2016).
- [16] L. Adamczyk *et al.* [STAR Collaboration], Phys. Rev. Lett. **113**, 092301 (2014).
- [17] L. Adamczyk *et al.* [STAR Collaboration], Phys. Rev. Lett. **112**, 032302 (2014).
- [18] M. M. Aggarwal *et al.* [STAR Collaboration], Phys. Rev. Lett. **105**, 022302 (2010).
- [19] B. Berdnikov and K. Rajagopal, Phys. Rev. D **61**, 105017 (2000).
- [20] P. Braun-Munzinger, K. Redlich and J. Stachel, In *Hwa, R.C. (ed.) et al.: Quark Gluon Plasma 3, 491–599 (2004).
- [21] J. Cleymans, H. Oeschler, K. Redlich and S. Wheaton, Phys. Rev. C **73**, 034905 (2006).
- [22] A. Andronic, P. Braun-Munzinger, K. Redlich and J. Stachel, J. Phys. G **38**, 124081 (2011).
- [23] V. V. Begun, M. I. Gorenstein, M. Hauer, V. P. Konchakovski and O. S. Zozulya, Phys. Rev. C **74**, 044903 (2006).
- [24] J. Fu, Phys. Lett. B **722**, 144 (2013).
- [25] F. Karsch and K. Redlich, Phys. Lett. B **695**, 136 (2011).
- [26] P. Garg, D. K. Mishra, P. K. Netrakanti, B. Mohanty, A. K. Mohanty, B. K. Singh and N. Xu, Phys. Lett. B **726**, 691 (2013).
- [27] P. Rau, J. Steinheimer, S. Schramm and H. Stcker, Phys. Lett. B **733**, 176 (2014).
- [28] P. K. Netrakanti, X. F. Luo, D. K. Mishra, B. Mohanty, A. Mohanty and N. Xu, Nucl. Phys. A **947**, 248 (2016).
- [29] D. K. Mishra, P. Garg and P. K. Netrakanti, Phys. Rev. C **93**, 024918 (2016).
- [30] G. D. Westfall, Phys. Rev. C **92**, 024902 (2015).
- [31] T. J. Tarnowsky and G. D. Westfall, Phys. Lett. B **724**, 51 (2013).
- [32] M. Nahrgang, M. Bluhm, P. Alba, R. Bellwied and C. Ratti, Eur. Phys. J. C **75**, no. 12, 573 (2015).
- [33] V. Koch, Chapter of the book "Relativistic Heavy Ion Physics", R. Stock (Ed.), Springer, Heidelberg, 2010, p. 626-652. (Landolt-Boernstein New Series I, v. 23).
- [34] S. Jeon and V. Koch, Phys. Rev. Lett. **83**, 5435 (1999).
- [35] M. Kitazawa and M. Asakawa, Phys. Rev. C **86**, 024904 (2012) Erratum: [Phys. Rev. C **86**, 069902 (2012)].